Journal of Materials Chemistry A

Accepted Manuscript

ROYAL SOCIETY OF CHEMISTRY

www.rsc.org/materialsA

Highly efficient macroporous adsorbents for toxic metal ions in water system based on polyvinyl alcohol-formaldehyde sponges

Yanxiong Pan, Zhi Liu, Weicai Wang, Chao Peng, Kai Shi, Xiangling Ji*

A series of macroporous adsorbents based on polyvinyl alcohol-formaldehyde (PVF) sponges was prepared using redox-initiated grafting polymerization of acrylamide (AM) and further hydrolysis under alkaline conditions. As-prepared sponges display average pore size in the range of 60-90 μm and interconnected pore with porosity approximately 90%. The elementary analysis confirmed that the amide groups in AM grafted PVF (PVF-g-GAM) have been rapidly converted into sodium carboxylate and the hydrolysis degree (*HD*) reaches approximately 65.5% within 6 h. The PVF-g-GAA (hydrolyzed PVF-g-GAM) sponges possesses excellent water absorption performance, such as ability to reach water absorption equilibrium within a few seconds and saturated absorption capacity more than 300 $g \cdot g^{-1}$. Importantly, the PVF-g-GAA can be used as adsorbents to remove toxic metal ions, such as Cu^{2+}, Pb^{2+} and Cd^{2+} ions in wastewater efficiently due to existence of abundant carboxyl in the above network. In single metal ion system, the sponges could reach adsorption equilibrium within 10 min and the adsorption kinetics fit with pseudo-second order kinetic equation well. The influence of pH and types of metal ions on the adsorption capacities are also investigated extensively. The PVF-g-GAA-20 displays high adsorption performance with maximum adsorption capacities for Cu^{2+}, Pb^{2+} and

Cd^{2+} up to 2.50, 3.20 and 3.15 mmol·g^{-1} at pH of 5.11, respectively. The equilibrium adsorption isotherm demonstrated that the adsorption equilibrium of PVF-g-GAA-20 for Cu^{2+}, Pb^{2+} and Cd^{2+} ions follows Langmuir isotherm model very well with maximum adsorption capacities approximately 4.00, 3.97 and 3.34 mmol·g^{-1}, respectively. In the binary metal ion coexistence system, including Cu^{2+}/Pb^{2+}, Cu^{2+}/Cd^{2+} and Pb^{2+}/Cd^{2+} mixtures, PVF-g-GAA-20 displayed excellent absorption selectivity for Cu^{2+} and Pb^{2+} and the values of $S_{Cd^{2+}}^{Cu^{2+}}$ and $S_{Cd^{2+}}^{Pb^{2+}}$ were 13.4 and 7.14, respectively. Notably, the adsorption capacities for the above three metal ions slightly decreased with the variation of ionic strength in the range of 0.01 to 0.08 M. The sample also exhibited quick desorption procedure less than 10 min and excellent reusability at least for six recycles. The adsorption mechanism was also discussed. Definitely, the PVF-g-GAA sponges are ideal adsorbents for removing/separating toxic metal ions in waste/polluted water body.

1. Introduction

Environmental pollutions from organic pollutants and toxic metal ions become two serious widespread pollutions in the water system to date. Most organic pollutants are readily evaporated and can be degraded in the environment, whereas toxic metal ions, such as Pb(II), Cd(II), Hg(II), Cu(II) and Cr(VI), possess obvious non-biodegradation and bioaccumulation.[1, 2] Given the catastrophic effect of toxic metal ions on the ecosystem and human health, the continuous monitoring and collection of pollutants from water are a great challenge to the researchers.[3-5] Various remediation methods such as membrane separation, precipitation, ion exchange, solvent extraction and

reverse osmosis process, are applied in waste water treatment. In particularly, the use of adsorbents is considered an efficient technique for removing toxic metal ions from the aqueous medium because of their numerous advantages such as high separation efficiency, easy operation, low cost and so on.

Materials with hydrophilic surface and functional groups, such as amines, carboxylic acids, amide, alcohol and thiourea, can be used as adsorbents for removal of toxic metal ions from water medium. The adsorbents can be classified into mineral, biological and organic materials based on different sources. Mineral nano-/micro-particles such as functionalized silica,[6-10] core-shell particle,[11, 12] metal oxide,[13-15] zeolite[16, 17], polyacrylamide-grafted carbonanotube[18] and graphene[19-21] exhibit rapid adsorption kinetics; however, the relatively low adsorption capacities (usually no more than 1 $mmol \cdot g^{-1}$) are the main drawback of these materials. Many biological adsorbents, including functionalized cellulose[22], chitosan,[23-25] fungi,[26, 27] and gelatin hydrogles,[28, 29] have been investigated for the adsorption of toxic metal ions as renewable source. For example, chitosan beads can adsorb Cu^{2+} approximately 2 $mmol \cdot g^{-1}$ in 10 min.[25] Compared with the mineral and biological source sorbents, organic adsorbents have flexible design and rich chemical compositions. Cation-exchange resin-supported Polyethyleneimine nanoclusters adsorbed Cu^{2+} about 1.5 $mmol \cdot g^{-1}$ in 240 min.[30] poly(glycidyl methacrylate-aspartic acid) resin adsorbs Cu^{2+} and Cd^{2+} about 1.2-1.4 $mmol \cdot g^{-1}$ in 40 min.[31] Aminated polyacrylonitrile fibers or nanocrystalline cellulose adsorbs Cu^{2+} about 0.3-0.5 $mmol \cdot g^{-1}$ in 120 min.[32, 33] polyvinyltetrazole-grafted polystyrene resin adsorbed Cu^{2+}, Pb^{2+}, Cr^{3+}, about 1.5-3.4 $mmol \cdot g^{-1}$ in 300-600 min.[34]

Hydrogels such as poly(acrylic acid-co-acrylamide), and xylan-rich hemicelluloses-graft-acrylic acid ionic hydrogels with excellent adsorption capacities

have been reported.[5, 35-37] For example, xylan-rich hemicellulose-based hydrogels can adsorb Pb^{2+} and Cd^{2+} up to 4.1 $mmol \cdot g^{-1}$ in 60 min.[36] Obviously, The disadvantages of these hydrogels including slow adsorption and desorption kinetics with at least a few hours or even days, limit their practical applications. Decrease the characteristic dimension through grinding as-prepared 3D hydrogel into powder specimens[38, 39] or prepared nano- or micro particles directly is a simple method to increase the adsorption rate.[40] In addition, introduction of porous structure is an effective strategy to enhance swelling-deswelling as well as adsorption and desorption rate of adsorbents because the diffusion-controlled swelling process of traditional hydrogel is changed into convection-controlled for porous adsorbents.[8, 22, 41] The interconnected and macroporous feature results adsorbent size that has almost no influence on the adsorption performance. More important, the porous monoliths facilitate to carry out the adsorption/desorption process before and after adsorption. Thus, an ideal adsorbent for toxic metal ions must exhibit the following characteristics: rapid adsorption kinetics in minute scale, high adsorption capacity up to $2mmol \cdot g^{-1}$, easy desorption procedure and excellent reusability.

Polyvinyl alcohol-formaldehyde (PVF) sponges are widely used as cleaning material in our daily lives and medical dressing because of their many advantages including good mechanical properties at low density, hydrophilic network, excellent water absorption capacity and biocompatibility. The existence of numerous hydroxyl groups in PVF foams enables to modify the surface property to obtain PVF sponges for different applications. In our previous work, facile post-modification and graft-polymerization were applied to prepare novel macroporous PVF sponges that exhibit good absorption for hydrocarbon pollutants[42, 43] or for water.[44] In present study, the macroporous hydrogels based on PVF sponges were successfully prepared via

graft polymerization of hydrophilic acrylamide (AM) on the PVF network and further hydrolysis under alkaline conditions. As-prepared samples used as efficient adsorbents for toxic metal ions were investigated extensively.

2. Experimental

2.1 Materials and Reagents

Poly (vinyl alcohol) (PVA) powder with a degree of polymerization 2000 and saponification degree of 99% was purchased from Shanxi Sanwei Group Co. Ltd., China. Triton X-100, glutaraldehyde (GA, 50% aqueous solution), ceric ammonium nitrate (CAN) and acrylamide (AM) were obtained from Aladdin. Formaldehyde (37% aqueous solution) and other reagents including sodium hydroxide, ethanol, concentrated sulfuric acid and disodium hydrogen phosphate were purchased from Beijing Chemical Works and used as received.

2.2 Preparation of Pristine Polyvinyl alcohol-formaldehyde (PVF) Sponge

A typical preparation of PVF sponge was reported in literature.[45] In detail, a certain amount of PVA was dissolved in 450 g hot water by vigorous stirring with magnetic stir bar at 95^{o}C until completely dissolution. Then, calculated formaldehyde and Triton X-100 were poured into 60 g of hot PVA solution under vigorous stirring. The liquid froths were obtained after 5 min, and then 30 mL of 50 wt% H_2SO_4 was poured into the above froth at room temperature. After reaching a maximum volume, the froths were poured into a mold and cured in an oven at 60^{o}C for 5 h. The raw samples were washed with water at least for five times to remove unreacted reactants. Finally, the sponge named as PVF with apparent density 0.073 g·cm^{-3} was available after drying at 60^{o}C to a constant weight.

2.3 Preparation of PVF-GA Sponge

The crosslinking reaction between hydroxyl groups in PVF network and glutaraldehyde (GA) was carried out in the presence of sulfuric acid as catalyst. Typically, 10 g of PVF sponge and 0.65 mL of GA (50% aqueous solution) were added into 400 mL of 20 wt% H_2SO_4 solution, the mixture was kept at 25°C for 24 h. Then, as-prepared sample was washed with water at least five times in order to remove sulfuric acid and unreacted GA completely and dried at 60°C to a constant weight, named as PVF-GA sponge with apparent density of 0.069 g·cm^{-3}.

2.4 Preparation of Macroporous PVF-g-GAM Sponges

Graft polymerization of AM monomer on the macroporous PVF-GA network was carried out using CAN as initiator under nitrogen atmosphere at room temperature.[46] Typically, 2 g PVF-GA sponge was swollen in 100 mL of 0.01 M nitric acid solution and kept for 0.5 h under nitrogen stream, then 20 mL 0.01 M nitric acid solution, and 0.559 g (0.001 mol) CAN and predetermined amount of AM, were added to the above mixture and stirred at 25°C for 24 h. Then, as-prepared samples were washed with deionized water/ethanol mixture to remove unreacted reactants and homopolymer, and dried in a vacuum oven at 60°C until constant weight was attained, and named as PVF-g-GAM-n, where n is the feed ratio of [AM]/[OH].

The grafting percentage (*GP*) and grafting efficiency (*GE*) of PVF-g-GAM were calculated using gravimetric method according to the following equations.

$$GP = (W_2\text{-}W_0)/W_0 \times 100\% \quad (1)$$

$$GE = (W_2\text{-}W_0)/W_1 \times 100\% \quad (2)$$

Where W_0, W_1 and W_2 were the weights (g) of pristine PVF-GA, AM and PVF-g-GAM after the polyacrylamide was removed, respectively.

The nitrogen content (*N*%) of as-prepared PVF-g-GAM was also measured and the *GP* and *GE* were also calculated through the following equations (see supporting

information, Part I).

$$GP = \frac{N\%}{0.197 - N\%} \times 100\% \qquad (3)$$

$$GE = \frac{W_2 \times N\%}{0.197 W_1} \times 100\% \qquad (4)$$

Where *N%* and N_1% were the nitrogen contents in PAM grafted and hydrolyzed samples, respectively.

2.5 Preparation of Macroporous PVF-g-GAA Sponges

The macroporous PVF-g-GAA-n sponges were available via the hydrolysis reaction of PVF-g-GAM-n in 1 M NaOH at 60^{o}C for 6 h. Then the hydrolyzed samples were washed with water/ethanol mixture thoroughly and dried in a vacuum oven at 60^{o}C, and named as PVF-g-GAA-n.

The hydrolysis degree of macroporous PVF-g-GAM in sodium hydroxide solution was also examined using elementary analysis, and calculated using the following equation

$$HD = \left(1 - \frac{23 + 14/N\%}{23 + 14/N_1\%}\right) \times 100\% \qquad (5)$$

where *N*%, N_1% were the nitrogen contents of as-prepared PVF-g-GAM-n and PVF-g-GAA-n, respectively.

2.6 Instruments and Characterization

Fourier transform infrared spectrum was measured on Bruker Vertex 70 spectrometer with attenuated total reflection (ATR) attachment. Solid-state CP/MAS ^{13}C-NMR was carried out on a Bruker AV-400-WB spectrometer. To verify the reliability of *GP* and *GE* obtained using gravimetric methods, the elementary analysis was run on an elementary vario EL instrument. For Scanning electron microscopy (SEM) test, the dried sponge was cut into sheet and immersed into liquid N_2 for 5 min,

then quickly broken off to get a random brittle-fractured surface and coated with a layer of gold for SEM observation, which were observed through a field-emission environmental SEM (Micro FEI Philips XL-30-ESEM-FEG) operating at 15 and 20 kV. Pore size and porosity were obtained by an automatic intrusion porosimeter (Autopore IV 9500, Micromeritics, USA). The concentration of toxic metal ions was diluted ten-fold and measured using inductively coupled plasma mass spectrometry (ICP-MS, Thermo Fisher Corp., USA). The surface element composition was determined by X-ray photoelectron spectroscopy (XPS) (VG ESCA MK II Thermo Avantage V 3.20 analyzer, with Al/K anode mono-X-ray source).

2.7 Water Absorption Performance

The gravimetric method was employed to investigate the swelling ratio of PVF-g-GAM-n and PVF-g-GAA-n at 25°C in deionized water and saline solution. At certain time intervals, the samples were taken out from the water (or saline solution) and the weights of wet sponges were determined after being drained for 0.5 min in stainless mesh. The absorption amount at time *t* (Q_t) was defined as

$$Q_t = (W_t - W_2)/W_2 \qquad (6)$$

where W_2 and W_t were the weights of dried sample and wet one at time *t*, respectively. The state of equilibrium swelling could be reached after 10 min and the saturated absorption capacity (Q_s) could be obtained as

$$Q_s = (W_s - W_2)/W_2 \qquad (7)$$

where W_s was the weight of wet sample at equilibrium.

2.8 Metal ions Adsorption Experiments

Adsorption of typically toxic metal ions (Cu^{2+}, Pb^{2+} and Cd^{2+}) in aqueous solution was carried out in batch adsorption experiments under room temperature (25°C). In the single metal ion system, 10 mg of PVF-g-GAA was added into 30 mL of solution

with metal ions in a 50 mL vial, and the pH values of initial solution were adjusted from 1.0 to 6.0 using 0.1 M HCl and 0.1 M NaOH solution, then continuous shaking at 120 rpm for 12 h and the final concentration of metal ion was analyzed using ICP-MS. In order to investigate the adsorption kinetics of PVF-g-GAA for metal ions, 100 mg of PVF-g-GAA was added into the 300 mL solutions with an initial concentration c_0 = 2.5 mM and pH = 5.11 under continuous shaking, 2.0 mL solution was taken out at certain interval for measurement of the metal ion concentration. The effect of metal ions concentration on the adsorption performance was also investigated at pH = 5.11, and then 10 mg of PVF-g-GAA was added into the solution with initial concentration of metal ions varying from 0.1 to 3.0 mM, the vials were shaken at 120 rpm for 12 h and the final metal ion concentration of each vial was analyzed. The adsorption capacity (q_e) was calculated using the following formula

$$q_e = (c_0\text{-}c_e)\times V\times 1000/W_2 \qquad (8)$$

where c_0 and c_e were the initial and final equilibrium metal ions concentration (mM) in solution, V was the volume of solution (mL), and the W_2 was the mass of dried PVF-g-GAA sample.

2.9 Adsorption Selectivity of PVF-g-GAA-20

In the binary metal ions system, the adsorption selectivity of PVF-g-GAA-20 was investigated. Typically, 10 mg of PVF-g-GAA-20 was added into the solutions containing 1.5 mM A ions and predetermined B ions (from 0.1 to 2.0 mM), and the ion concentration in the solution was analyzed after shaking at 120 rpm for 12 h. The ratio of q_e (A)/q_e (B) was used to indicate selectivity S_B^A ,[47, 48]

$$S_B^A = \frac{q_e(A)}{q_e(B)} \qquad (9)$$

where q_e (A) and q_e (B) were the saturated adsorption capacities of adsorbents for the metal ions with a stronger and a weaker affinity.

The influence of Cd^{2+} on the adsorption capacities was also investigated as mentioned above. The influence of ion strength, adjusting from 0.02 to 0.1 M using 0.5 M NaCl, on the adsorption performances was also examined.

Desorption and Reusability of PVF-g-GAA-20

PVF-g-GAA-20 saturated with metal ions, was added into the 0.1 M HCl solution shaking for 30 min, and subsequently immersed into the 0.1 M $NaHCO_3$ for 20 min to convert the -COOH to the $-COO^-Na^+$. Then the PVF-g-GAA-20 was picked up from the solution and washed with deionized water/ethanol mixture at least three times, and dried in a vacuum oven at 60°C to a constant weight. Six cycles of adsorption-desorption were performed for the reusability of this sample.

3. Results and discussion

3.1 Characterization of Chemical Composition and Pore Structures

Figure 1 shows the FTIR spectra of PVF, PVF-g-GAM-20 and PVF-g-GAA-20. For pristine PVF sponge, the broad absorption peak at 3200-3600 cm^{-1} and the peak at 2843-2943 cm^{-1}, are attributed to the O–H stretching vibration and C–H stretching vibrations of the alkyl groups, respectively. The absorption peak at 1060 cm^{-1} reveals the existence of OH in PVF network. For PVF-g-GAM-20, the appearance of double peaks at 3427 cm^{-1} and 3195 cm^{-1} is due to the N-H asymmetric and N-H symmetric stretching vibration of the NH_2 group of PAM, and the new peaks at 1672 cm^{-1} and 1610 cm^{-1} were attributed to the C＝O stretching vibration of AM. These peaks confirm the successful grafting of polyacrylamide on the surface of macroporous PVF. The relative increase of the typical peaks of PVF-g-GAA-20 at 3427 cm^{-1} for O-H stretching vibration, appearance of new peak at 1565 cm^{-1} for asymmetric stretching vibration of carboxylate anion in PVF-g-GAA-20, and the existence of C=O

stretching vibration of acrylamide at 1671 cm^{-1}, respectively, confirmed that the amide groups of PVF-g-GAM 20 are partially converted to the carboxylate groups under basic conditions.

The pore size and distribution of these sponges are characterized using mercury intrusion porosimeter as shown in Figure 2. The pristine PVF and PVF-g-GAM-20 roughly exhibit unimodal macroporous size distribution with a peak centered at about 60 μm and 90 μm because of the limitation of mercury porosimetry at low pressure as well as the nature of sample.[49] The PVF-g-GAA-20 displayed similar pore size and distribution as pristine PVF. The porosities of PVF, PVF-g-GAM-20 and PVF-g-GAA-20 are 95.0%, 88.8% and 91.9%, respectively. This result demonstrates that the sponges maintained interconnected pore structure and high porosity after successive grafting polymerization and hydrolysis. As shown in Figure 3, the SEM images also confirm that all samples exhibit a macroscopic rough surface and interconnected pore structure. The pore size spans from a few micrometers to 200 μm like pristine PVF, which benefits to a rapid convection of solvents and reagents in the polymer networks.[50]

3.2 Hydrolysis Kinetics of PVF-g-GAM Sponges

Generally, PAM is easily hydrolyzed under acidic or basic conditions.[51, 52] Figure 4 shows a typically hydrolyzed process of PVF-g-GAM-20 under alkaline condition. The process could be divided into two stages. Stage I has a rather quickly hydrolyzed rate and the hydrolysis degree (*HD*) could reach 47.6% within initial 1 hour, and the corresponding nitrogen content of the sample rapidly decreases from 14.1% to 6.6%, which is higher than that of pure polyacrylamide or polyacrylamide hydrogel in alkaline solution.[53] Such rapid hydrolysis kinetics at the initial stage was attributed to the synergistic effect of interconnected pore structure of PVF-g-GAM and the

catalytic effect of the neighboring amide group.[51, 52] Stage II has a relatively slow rate and the conversion degree gradually increases with the reaction time, correspondingly, the sample reaches hydrolysis equilibrium. When the reaction time was extended to 6 h, the nitrogen content is 4.21% and *HD* is 65.5%, respectively. The slow hydrolysis rate is attributed to the enhanced electrostatic repulsion between the OH^- ions of alkaline and the accumulating carboxylate anions COO^- in the polymer chain of sample, this phenomenon generates a strong electrostatic repulsion effect, as a consequence, causing a progressive decrease on the hydrolysis rate. For the sample reacted for 24 h, the nitrogen content is 3.6% and *HD* is 70.4%, respectively, indicating only a slight increase in *HD* with extension of reaction time.

3.3 Water Absorption Performance

As shown in Figure 5, the pristine PVF reaches water absorption equilibrium in 120 s, PVF-g-GAM-20 and PVF-g-GAA-20 exhibits a relatively more rapid absorption kinetics in 60 s, which is much higher than most superabsorbents.[22, 41, 54] The quicker absorption kinetics of grafted and hydrolyzed samples for water is mainly ascribed to the existence of hydrophilic amide and COO^- groups in the networks, respectively, which can improve surface wettability and accelerate the penetrating kinetics of water molecules into the sponges. Figure 5 also reveals the saturated absorption capacities (Q_s) of sponges for water; for example, the Q_s of PVF-g-GAM-20 is 44.1 $g \cdot g^{-1}$, which is higher than 20.0 $g \cdot g^{-1}$ of pristine PVF due to the contribution of solvation effect of hydrophilic PAM segments. The Q_s of PVF-g-GAA-20 in deionized water is 315.2 $g \cdot g^{-1}$, approximately 8-15 times that of pristine PVF and PVF-g-GAM-20. Such high absorption capacity is attributed to the existence of numerous negative COO^- groups in the network of PVF sponge. Consequently, the osmotic pressure difference between PVF network and external water promotes the polymer chain expansion, while the

repulsive interactions between the chains enhanced the solvation degree of PVF-g-GAA-20 network effectively.

3.4 Adsorption Kinetics and Adsorption Capacity in Single Metal Ion System

As-prepared PVF-g-GAA-20 sponge can be used as efficient adsorbents for toxic metal ions owing to its hydrophilic surface[55, 56] and the existence of lot of $–COO^-$ and $–CONH_2$ in the network of samples.[57] Here, Cu^{2+}, Pb^{2+} and Cd^{2+} were selected as typical toxic metal ions for a series of study.

(i) Adsorption Kinetics

Figure 6 shows the adsorption kinetic curves and fitted results of PVF-g-GAA-20 for Cu^{2+}, Pb^{2+} and Cd^{2+} at pH = 5.11. The adsorption rates for Cu^{2+}, Pb^{2+} and Cd^{2+} on the sponges increase rapidly, and could reach adsorption equilibrium within approximately 10 min, indicating the superfast adsorption kinetics. As shown in Figure 6a and Table 1, the adsorption kinetics was investigated by using the pseudo-first-order model, its equation is expressed as follows

$$q_t = q_e(1-e^{-K_1 t}) \qquad (10)$$

where q_e and q_t are the adsorption capacities at equilibrium and time t, respectively, and K_1 is the adsorption constant. The fitted q_e values of the sample for Cu^{2+}, Pb^{2+} and Cd^{2+} are 2.47, 3.20 and 3.07 $mmol \cdot g^{-1}$, respectively, which are closed to the corresponding experimental results of 2.50, 3.26 and 3.15 $mmol \cdot g^{-1}$, and K_1 values are 0.45, 0.52 and 0.33 min^{-1} with correlation coefficient of $R^2 \geq 0.9879$. The adsorption kinetics was also investigated by using pseudo-second-order models, which is given as

$$\frac{t}{q_t} = \frac{1}{K_2 q_e^2} + \frac{t}{q_e} \qquad (11)$$

Where q_e and q_t are the adsorption capacities at equilibrium and time t, and the K_2 are

the adsorption constant of pseudo-second-order models. The fitted q_e values of the sample for Cu^{2+}, Pb^{2+} and Cd^{2+} are 2.54, 3.26 and 3.22 $mmol \cdot g^{-1}$, respectively, which are similar to the experimental results. The K_2 for Cu^{2+}, Pb^{2+} and Cd^{2+} are 0.16, 0.32 and 0.13 $g \cdot mmol^{-1} \cdot min^{-1}$ with higher $R^2 \geq 0.9996$ respectively. These results indicate that the adsorption kinetics could be better described using pseudo-second-order models. Notably, the adsorption kinetics are equivalent to or higher than most other adsorbents such as particles and membranes, urchin-like Ni–P microstructures,[58] L-cysteine functionalized multi-walled carbon nanotubes,[59] mesoporous poly-melamine-formaldehyde polymer,[4] iron nanoparticles[56] and thiol-functionalized Zn-doped biomagnetite particles.[60] The aforementioned results demonstrate that the PVF-g-GAA-20 exhibited rapid adsorption kinetics and higher adsorption capacities. The adsorption process in Cu^{2+} solution demonstrated the rapid adsorption characteristics of PVF-g-GAA-20 for toxic metal ions, as shown in Figure 7 (see details in the ESI, Movie I†). The PVF-g-GAA-20 sponge could reach swelling equilibrium in the copper solution in 1 minute, and then the sponge dimension gradually decreases with time, and the color of sponge gradually becomes blue due to the adsorption of abundant Cu^{2+} ions on the sponge network. The rapid swelling kinetics and high swelling degree of PVF-g-GAA-20 rendered the adsorption sites on the polymer networks adequately available at the initial stage. The toxic metal ions in the solution could then be anchored onto the polymeric network within a short time. The swelling degree of the sample decreases with contact time because of the attachment of metal ions on the adsorption sites, which has a negative effect on the repulsion between polymer chains and the osmotic pressure difference between interior and exterior of polymer network. It should be mentioned that the removal of adsorbents from metal ion solution can be easily achieved using a forceps.

(ii) Influence of pH Value of Metal Ion Solutions on Adsorption Capacity

In Figure 8a, the adsorption capacities of PVF-g-GAA-20 for Cu^{2+}, Cd^{2+} and Pb^{2+} increase rapidly with pH in the range of 1.6-3.0, respectively, but further increasing the initial pH of solutions results in a plateau in the adsorption capacity besides Pb^{2+} system because of Pb^{2+} precipitation formation at higher pH value. For example, the adsorption capacity of PVF-g-GAA-20 for Cu^{2+} increases from 0.043 $mmol \cdot g^{-1}$ at pH=1.65 to 3.21 $mmol \cdot g^{-1}$ at pH=6.5, demonstrating that the pH value has significant influence on the adsorption capacities for metal ions. To investigate the reasons for the above results, we monitor the zeta potentials of PVF-g-GAA-20 at different pH values as shown in Figure 8b. The zeta potential is positive at pH $<$ 2.0 whereas negative at pH $>$ 2.0, which is probably attributed to the formation of protonated AM of non-ionic PAM chains at lower pH values.[4] Simultaneously, the COO^- ions in the PVF-g-GAA-20 network becomes COOH groups at lower pH value.[61] In addition, the zeta potential decrease from 0 mV at pH = 2.0 to approximately -25 mV at pH = 8.7 due to the generation of more COO^- in the networks, which indicates more available sites for adsorption of toxic metal ions.

(iii) Saturated Adsorption Capacity and Adsorption Isotherm

Figure 9 shows the adsorption capacities in Cu^{2+}, Pb^{2+} and Cd^{2+} solutions at different initial concentrations. The contact time selected was 12 h to ensure sufficient time to reach adsorption equilibrium. At a lower initial ion concentration (C_0), particularly in the range of 0.1-1.5 mM (the corresponding C_e in the solution after reaching adsorption equilibrium is 0-0.25 mM), the q_es rapidly increase with C_0. At a relatively high initial ion concentration, that is, $C_0 \geq 2.0$ mM (correspondingly $C_e \geq 0.94$ mM for Cu^{2+} solution), only a slight increase in q_e is observed. The above adsorption

behaviors for metals ions are fitted with the Freundlich and Langmuir model according to the following formula as:

$$q_e = K_F C_e^{1/n} \quad (12)$$

$$\frac{C_e}{q_e} = \frac{1}{q_{max} K} + \frac{C_e}{q_{max}} \quad (13)$$

where K_F is the Freundlich adsorption equilibrium constant, and 1/n is generally from 0 to 1. C_e and q_e are the equilibrium concentration of metal ions in solution and saturated adsorption amount for metal ions, and K is the Langmuir isotherm constant (Figure 9 and Table 1). The correlation coefficients $R^2 \leq 0.880$ using Freundlich model and $R^2 \geq 0.977$ using Langmuir model, indicate that the Langmuir isotherm model is more suitable for fitting the experimental data and the formation of monolayer coverage on the adsorbent surface after adsorbing toxic metal ions. The q_ss of PVF-g-GAA-20 in Cu^{2+}, Pb^{2+} and Cd^{2+} solutions are predicted to be 4.00, 3.97 and 3.34 mmol·g^{-1}, respectively, which is higher than most of adsorbents, as shown in Table 2.

3.5 Adsorption Selectivity in Binary Metal Ions System

The adsorption performance in the binary metal ions system is shown in Figure 10. For example, at the fixed initial concentration of $c_{0\,[Pb^{2+}]}$ = 1.5 mM (Figure 10a), the q_e of PVF-g-GAA-20 for Pb^{2+} only decreases gradually from 2.91 to 1.60 mmol·g^{-1} with the increase of $c_{0\,[Cu^{2+}]}$ from 0.1 to 2.0 mM. Conversely, that q_e for Cu^{2+} decreases from 2.41 to 0.56 mmol·g^{-1}, implying that PVF-g-GAA-20 possesses better adsorption selectivity for Pb^{2+} than Cu^{2+} in the Cu^{2+}/Pb^{2+} mixtures. On the other hand, the coexistence of multiple metal ions negatively influence the saturated adsorption capacity q_e for one metal ion because the adsorption selectivity and adsorption

capacity are concentration-dependent.[57] In the other coexistence systems, such as Cu^{2+}/Cd^{2+} and Pb^{2+}/Cd^{2+} mixtures, as shown in Figure 10b and 10c, PVF-g-GAA-20 exhibits better adsorption selectivity for Cu^{2+} and Pb^{2+}, respectively. In general, the adsorption selectivity can be simply expressed by the selectivity coefficient (S_B^A) as shown in equation (9). Here, the values of $S_{Cu^{2+}}^{Pb^{2+}}$, $S_{Cd^{2+}}^{Cu^{2+}}$ and $S_{Cd^{2+}}^{Pb^{2+}}$ in the Cu^{2+}/Pb^{2+}, Cu^{2+}/Cd^{2+}, and Pb^{2+}/Cd^{2+} mixtures are 2.17, 13.4 and 7.14, respectively, which is probably attributed to the differences of hydration energy and hydrated ionic radius between the toxic metal ions.[62] The above results demonstrate that Cu^{2+} and Pb^{2+} are preferentially adsorbed species in the Cu^{2+}/Cd^{2+} and Pb^{2+}/Cd^{2+} mixtures, respectively, while the selective adsorption of Cu^{2+}/Pb^{2+} mixture is unsatisfactory. It means that as-prepared adsorbent can be used as effective separation material to realize the roughly separation of Cu^{2+} or Pb^{2+} from the Cu^{2+}/Cd^{2+} or Pb^{2+}/Cd^{2+} mixture.

In general, the ion strength of solution also influences the adsorption capacity for toxic metal ions. Here, the metal ion strength is the sum of Cu^{2+}, Pb^{2+}, Cd^{2+} and Na^{+} (NaCl as a major adjuster for ion strength). In Figure 11, when the ionic strength increases from 0.01 to 0.08 M, adsorption capacity for Cu^{2+} decreases from 3.14 to 2.61 mmol·g^{-1}, whereas that for Pb^{2+} evidently decreases from 3.49 to 1.44 mmol·g^{-1}, demonstrating that adsorption capacity decreased with ionic strength. However, the adsorption capacity for Cd^{2+} exhibits slight change between 2.87 and 3.10 mmol.g^{-1} with ionic strength. These features can be attributed to the following factors. At a relative lower concentration of competition ions (in here is Na^{+}), the toxic metal ions tend to form outer-sphere complexes with the active sites in the PVF-g-GAA-20, and the sponge exhibit a relative higher q_s. Limited swelling of macroporous PVF-g-GAA-20 in the solution under relatively higher ionic strength reduced the binding of toxic metal ions with the active sites of the sample. Simultaneously, the

existence of NaCl in the solution also negatively affects the diffusion of metal ions into the polymer networks. As reported in literature, the adsorption procedure is possibly ion-exchange procedure.[63, 64]

3.6 Desorption of Adsorbed Metal Ions and Reusability of Sponges

The reusability of adsorbent is an important factor to determine its practical applications. Desorption experiment was successfully carried out by a two-step elution using 0.1 M HCl and 0.1 M $NaHCO_3$ to regenerate adsorbed macroporous PVF-g-GAA-20 sponge. PVF-g-GAA-20 exhibits higher desorption rate as shown in Figure12 (see details in the ESI, Movie II†). Once PVF-g-GAA-20-Cu, that is, PVF-g-GAA-20 saturated with Cu^{2+}, was immersed into the 0.1 M HCl solution in a few minutes, the blue color of the sample rapidly disappeared, indicating that the sample can reach desorption equilibrium only within a few minutes due to its open-cell structure and high porosity. Absolutely, its desorption procedure is better than many adsorbents, such as traditional hydrogels[28-29] or particles[48, 57] which generally need a few hours or days to reach desorption equilibrium.

The reusability of PVF-g-GAA-20 for Cu^{2+}, Pb^{2+} and Cd^{2+} is shown in Figure 13. The adsorption capacities of PVF-g-GAA-20 for Cu^{2+} are 2.74, 2.75, 2.78, 2.76, 2.89 and 3.20 $mmol \cdot g^{-1}$, corresponding to the 1st, 2nd, 3rd, 4th, 5th, 6th cycle, which indicates the adsorption capacities of sample for Cu^{2+} slightly fluctuated after six cycles of adsorption-desorption. Actually, the sample also exhibits similar adsorption performance for Pb^{2+} and Cd^{2+} systems, and the saturated adsorption capacities for Pb^{2+} are within the range of 2.88 and 3.07 $mmol \cdot g^{-1}$ while those for Cd^{2+} are within the range of 2.61 and 3.21 $mmol \cdot g^{-1}$. Such excellent adsorption reusability is attributed to the existence of numerous active groups in the PVF-g-GAA-20 and its good mechanical properties after pre-crosslinking with glutaradehyde.[31] The slight

increase of adsorption capacity for Cu^{2+}, Cd^{2+} and Pb^{2+} in the next cycle is probably due to the further hydrolysis of residual amide groups after recycle experiments, which would increase the amount of sodium polyacrylate in the sponge network.

3.7 Adsorption Mechanism

X-ray photoelectron spectra (XPS) were exploited to study the chemical composition and identify the interaction of metal ions with the related groups in the samples. Figure S3 exhibits the XPS survey spectra of PVF, PVF-g-GAM-20 and PVF-g-GAA-20 before and after Cu^{2+} and Pb^{2+} adsorption. The two peaks at 532.4 eV and 533.6 eV come from **O**CH_2**O** and **O**H in PVF, and the two strong peaks at 531.5 eV and 533.4 eV are attributed to the **O**CH_2**O** and C=**O** in PVF-g-GAM. After hydrolysis under alkaline condition, a new peak appears at 530.8 eV due to (CO)**O** in PVF-g-GAA, which implies that the hydrolyzed sample was obtained. The appearance of new single peak at 399.2 eV from the N1s of amide further confirms that the polyacrylamide chains are grafted onto the macroporous PVF network. Meanwhile, the decrease of intensity after hydrolysis indicates that the PVF-g-GAA-20 are hydrolyzed partly. The new peaks at 933.8 eV and 138.4 eV are assigned to $Cu2p_{3/2}$ and $Pb4f_{7/2}$, indicating successful adsorption of Cu^{2+} and Pb^{2+} on the PVF-g-GAA-20 networks. As shown in Figure 14a, O1s of PVF-g-GAA-20 locates at about 531.5 eV and 533.4 eV, O1s of PVF-g-GAA-20-Cu could be fitted by two peaks at about 531.5 eV and 533.0 eV, while that of PVF-g-GAA-20-Pb is at 531.3 eV and 532.8 eV, respectively. The variation of the peak position suggests the formation of Cu-O and Pb-O bond, respectively.[49] The single peak at 933.7 eV is a characteristic peak of Cu-O bonding, implying the effective Cu^{2+} adsorption on PVF-g-GAA-20, which are mainly attributed to the coordination between Cu^{2+} and the oxygen atom of acrylic acid. Similarly, PVF-g-GAA-20 saturated with Pb^{2+}

displays a strong peak at 138.6 eV, indicating the formation of Pb-O between Pb^{2+} and oxygen atom of acrylic acid. The PVF-g-GAA-20-Cu^{2+} or Pb^{2+} also exhibit similar peaks at about 399.5 eV, indicating that toxic metal ion has no influence on the reduction of electron cloud density of the nitrogen atom,[57] and that the nitrogen atoms of amide are not involved in adsorption process.

The adsorption mechanism of PVF-g-GAA-20 for Cu^{2+} and Pb^{2+} can also be confirmed by FTIR spectra. As shown in Figure 14b, after adsorption of Cu^{2+} and Pb^{2+}, the C=O vibration of amide in PVF-g-GAA-20 slightly shifts from 1672 cm^{-1} to 1666 and 1667 cm^{-1}, respectively, while the asymmetric stretching vibration of $-COO^-$ at 1565 cm^{-1} is displaced by 1604 cm^{-1} (PVF-g-GAA-20-Cu) and 1532 cm^{-1} (PVF-g-GAA-20-Pb) with a relatively lower intensity, which indicates that the adsorption of PVF-g-GAA-20 for the above two ions is mainly determined by the carboxylate groups of sponges.

The adsorption of toxic metal ions onto the network of PVF-g-GAA-20 changes the surface morphology of sample to some extent, as shown in the enlarged view of local structure in Figure 14c. PVF-g-GAA-20 shows a relatively smooth surface, whereas PVF-g-GAA-20-Cu and PVF-g-GAA-20-Pb possessed abundant apophyses with a few hundred nanometers, resulting in a rough surface, which is attributed to the aggregation of a great deal of toxic metal ions on the sponge surface. Correspondingly chemical composition analysis from EDAX spectra (Figure 14c) revealed that C, O and Na were the dominant components in the network of PVF-g-GAA-20, whereas Cu^{2+} and Pb^{2+} became one of the dominant components of PVF-g-GAA-20-Cu and PVF-g-GAA-20-Pb, respectively. it was noted that the peak intensity of Na^+ obviously decrease after adsorption Cu^{2+} and Pb^{2+}, confirming the bonding with carboxylate groups is probably attributed to the high adsorption performance of

sample for toxic metal ions. Definitely, open-cell structure, high porosity, strong interaction between carboxylate groups and metal ions, and apophyses on the surface contribute a synergetic effect on the final adsorption performance.

4. Conclusions

Novel macroporous PVF-g-GAA sponges were successfully prepared via the redox grafting polymerization of AM and further hydrolysis under alkaline condition. With regard to the structure, water absorption, adsorption for toxic metal ions, the following conclusions are summarized.

i. As-prepared sponges possess interconnected pore structure and high porosity up to 90%. They exhibited rapid absorption kinetics for water and could reach absorption equilibrium within 60 s and, the absorption capacity could reach 315.2 $g \cdot g^{-1}$.

ii. As-prepared sponges can adsorb toxic metal ions including Cu^{2+}, Pb^{2+} and Cd^{2+} ions from the water medium and reach adsorption equilibrium within 10min. The absorption kinetics fit with pseudo-second order kinetics equation very well and the saturated adsorption capacities of PVF-g-GAA-20 for above three ions are 2.50, 3.26 and 3.15 $mmol \cdot g^{-1}$, respectively. The Langmiur model is suitable to fit the experimental data of the isotherm adsorption process, and the fitted q_m for Cu^{2+}, Pb^{2+} and Cd^{2+} were 4.00, 3.97 and 3.34 $mmol.g^{-1}$, respectively.

iii. In binary metal ions system, the PVF-g-GAA-20 exhibits excellent selectivity, $S_{Cd^{2+}}^{Cu^{2+}} > S_{Cd^{2+}}^{Pb^{2+}} > S_{Cu^{2+}}^{Pb^{2+}}$ for the Cu^{2+}/Cd^{2+}, Pb^{2+}/Cd^{2+}, and Pb^{2+}/Cu^{2+} mixtures. Even in the presence of NaCl, the sponge still displays good preferential adsorption feature for toxic Cu^{2+}, Cd^{2+}, and Pb^{2+} ions. The sponge

also exhibits rapid desorption kinetics in 10 min through a sequential immersion in HCl and $NaHCO_3$ solutions. Excellent reusability is also available.

iv. The adsorption mechanism is proposed. Such open-cell structure, high porosity, strong interaction between carboxylate groups and metal ions, apophyses on surface contribute a synergetic effect on the final excellent adsorption performance.

v. This kind of macroporous sponges overcome the drawback of traditional hydrogels and are an ideal adsorbent candidate for the removal and separation of toxic metal ions from the waste/polluted water body.

5. Acknowledgements

This research was supported by National Natural Science Foundation of China (General: 51173180) and Department of Science and Technology of Jilin Province (20130206057GX).

6. Notes and references

State Key Laboratory of Polymer Physics and Chemistry, Changchun Institute of Applied Chemistry, Chinese Academy of Sciences, Changchun 130022, P. R. of China
*Email: xlji@ciac.ac.cn. Tel: +86-431-85262876; Fax: +86-431-85262075

Supporting information: the calculation equation of *GP*, *GE* and *HD* using the elementary analysis, XPS survey scanning of PVF, PVF-g-GAM-20, PVF-g-GAA-20,PVF-g-GAA-20-Cu, PVF-g-GAA-20-Pb as well as the N and O assignments for PVF, PVF-g-GAM-20, PVF-g-GAA-20, the rapid adsorption (Movie

I with double speed) and desorption (Movie II with fourfold speed) procedures. This information is available free of charge via the Internet at http://pubs.rsc.org.

1. J. O. Duruibe, M. O. C. Ogwuegbu and J. N. Egwurugwu, *Int. J. Phys. Sci.*, 2007, **2**, 112-118.
2. L. Cui, J. Wu and H. Ju, *ACS Applied Materials & Interfaces*, 2014, **6**, 16210-16216.
3. M. Teresa Albelda, J. C. Frias, E. Garcia-Espana and H.-J. Schneider, *Chemical Society Reviews*, 2012, **41**, 3859-3877.
4. M. X. Tan, Y. N. Sum, J. Y. Ying and Y. Zhang, *Energy & Environmental Science*, 2013, **6**, 3254-3259.
5. A. P. Esser-Kahn, A. T. Iavarone and M. B. Francis, *Journal of the American Chemical Society*, 2008, **130**, 15820-15822.
6. H. S. Jung, M. Park, J. H. Han, J. H. Lee, C. Kang, J. H. Jung and J. S. Kim, *Chemical Communications*, 2012, **48**, 5082-5084.
7. A. Sinha and N. R. Jana, *Chemical Communications*, 2012, **48**, 9272-9274.
8. Z. Wu and D. Zhao, *Chemical Communications*, 2011, **47**, 3332-3338.
9. J. Liu and X. Du, *Journal of Materials Chemistry*, 2011, **21**, 6981-6987.
10. S. J. L. Billinge, E. J. McKimmy, M. Shatnawi, H. J. Kim, V. Petkov, D. Wermeille and T. J. Pinnavaia, *Journal of the American Chemical Society*, 2005, **127**, 8492-8498.
11. L. Zhao, H. Liu, F. Wang and L. Zeng, *Journal of Materials Chemistry A*, 2014, **2**, 7065-7074.
12. S.-H. Huang and D.-H. Chen, *Journal of Hazardous Materials*, 2009, **163**, 174-179.
13. C. L. Warner, R. S. Addleman, A. D. Cinson, T. C. Droubay, M. H. Engelhard, M. A. Nash, W. Yantasee and M. G. Warner, *Chemsuschem*, 2010, **3**, 749-757.
14. X. Yang, X. Wang, Y. Feng, G. Zhang, T. Wang, W. Song, C. Shu, L. Jiang and C. Wang, *Journal of Materials Chemistry A*, 2013, **1**, 473-477.
15. X. Wang, J. Cai, Y. Zhang, L. Li, L. Jiang and C. Wang, *Journal of Materials Chemistry A*, 2015, **3**, 11796-11800.
16. U. Wingenfelder, C. Hansen, G. Furrer and R. Schulin, *Environmental Science & Technology*, 2005, **39**, 4606-4613.
17. U. Wingenfelder, B. Nowack, G. Furrer and R. Schulin, *Water Research*, 2005, **39**, 3287-3297.
18. S. Yang, J. Hu, C. Chen, D. Shao and X. Wang, *Environmental Science & Technology*, 2011, **45**, 3621-3627.
19. S. Yang, C. Chen, Y. Chen, J. Li, D. Wang, X. Wang and W. Hu, *ChemPlusChem*, 2015, **80**, 480-484.
20. H. Chang and H. Wu, *Energy & Environmental Science*, 2013, **6**, 3483-3507.
21. S. Yang, C. Chen, Y. Chen, J. Li, D. Wang, X. Wang and W. Hu, *ChemPlusChem*, 2015, **80**, 480-484.
22. C. Chang, B. Duan and L. Zhang, *Polymer*, 2009, **50**, 5467-5473.
23. Y. Chen, L. Chen, H. Bai and L. Li, *Journal of Materials Chemistry A*, 2013, **1**, 1992-2001.
24. Z. Liu, H. Wang, C. Liu, Y. Jiang, G. Yu, X. Mu and X. Wang, *Chemical Communications*, 2012, **48**, 7350-7352.
25. W. Jiang, W. Wang, B. Pan, Q. Zhang, W. Zhang and L. Lv, *Acs Applied Materials &*

Interfaces, 2014, **6**, 3421-3426.
26. S. B. Deng and Y. P. Ting, *Environmental Science & Technology*, 2005, **39**, 8490-8496.
27. A. Naeem, J. R. Woertz and J. B. Fein, *Environmental Science & Technology*, 2006, **40**, 5724-5729.
28. C. Li, S. Yanagisawa, B. M. Martins, A. Messerschmidt, M. J. Banfield and C. Dennison, *Proceedings of the National Academy of Sciences*, 2006, **103**, 7258-7263.
29. Q. Xing, K. Yates, C. Vogt, Z. Qian, M. C. Frost and F. Zhao, *Sci. Rep.*, 2014, **4**.
30. Y. Chen, B. Pan, H. Li, W. Zhang, L. Lv and J. Wu, *Environmental Science & Technology*, 2010, **44**, 3508-3513.
31. C.-Y. Chen, M.-S. Lin and K.-R. Hsu, *Journal of Hazardous Materials*, 2008, **152**, 986-993.
32. A. Sheikhi, S. Safari, H. Yang and T. G. M. van de Ven, *Acs Applied Materials & Interfaces*, 2015, **7**, 11301-11308.
33. S. Deng, Bai and J. P. Chen, *Langmuir*, 2003, **19**, 5058-5064.
34. Y. Chen, M. He, C. Wang and Y. Wei, *Journal of Materials Chemistry A*, 2014, **2**, 10444-10453.
35. X.-W. Peng, J.-L. Ren, L.-X. Zhong, F. Peng and R.-C. Sun, *Journal of Agricultural and Food Chemistry*, 2011, **59**, 8208-8215.
36. X.-W. Peng, L.-X. Zhong, J.-L. Ren and R.-C. Sun, *Journal of Agricultural and Food Chemistry*, 2012, **60**, 3909-3916.
37. E. Orozco-Guareño, F. Santiago-Gutiérrez, J. L. Morán-Quiroz, S. L. Hernandez-Olmos, V. Soto, W. d. l. Cruz, R. Manríquez and S. Gomez-Salazar, *Journal of Colloid and Interface Science*, 2010, **349**, 583-593.
38. X. Zheng, D. Wu, T. Su, S. Bao, C. Liao and Q. Wang, *ACS Applied Materials & Interfaces*, 2014, **6**, 19840-19849.
39. L. Yu, X. Liu, W. Yuan, L. J. Brown and D. Wang, *Langmuir*, 2015, **31**, 6351-6366.
40. H. Kaşgöz, A. Durmuş and A. Kaşgöz, *Polymers for Advanced Technologies*, 2008, **19**, 213-220.
41. L. Yin, L. Fei, F. Cui, C. Tang and C. Yin, *Biomaterials*, 2007, **28**, 1258-1266.
42. Y. Pan, K. Shi, C. Peng, W. Wang, Z. Liu and X. Ji, *ACS Applied Materials & Interfaces*, 2014, **6**, 8651-8659.
43. Y. Pan, W. Wang, C. Peng, K. Shi, Y. Luo and X. Ji, *RSC Advances*, 2014, **4**, 660-669.
44. Y. Pan, K. Shi, Z. Liu, W. Wang, C. Peng and X. Ji, *RSC Advances*, 2015, **5**, 78780-78789.
45. H. G. Hammond, *US 2668153*, 1953.
46. G. Fundueanu, M. Constantin and P. Ascenzi, *Acta biomaterialia*, 2010, **6**, 3899-3907.
47. V. J. Inglezakis, M. D. Loizidou and H. P. Grigoropoulou, *Journal of Colloid and Interface Science*, 2003, **261**, 49-54.
48. L. Lv, M. P. Hor, F. Su and X. S. Zhao, *Journal of Colloid and Interface Science*, 2005, **287**, 178-184.
49. H. Giesche, *Particle & Particle Systems Characterization*, 2006, **23**, 9-19.
50. J. Chen, H. Park and K. Park, *Journal of Biomedical Materials Research*, 1999, **44**, 53-62.
51. K. Nagase and K. Sakaguchi, *Journal of Polymer Science Part A: General Papers*, 1965, **3**, 2475-2482.
52. S. Sawant and H. Morawetz, *Macromolecules*, 1984, **17**, 2427-2431.
53. V. F. Kurenkov, H. G. Hartan and F. I. Lobanov, *Russian Journal of Applied Chemistry*, 2001,

74, 543-554.

54. S.-L. Loo, W. B. Krantz, T.-T. Lim, A. G. Fane and X. Hu, *Soft Matter*, 2013, **9**, 224-234.
55. I. Ali, *Chemical Reviews*, 2012, **112**, 5073-5091.
56. P. Huang, Z. Ye, W. Xie, Q. Chen, J. Li, Z. Xu and M. Yao, *Water Research*, 2013, **47**, 4050-4058.
57. N. Li, R. B. Bai and C. K. Liu, *Langmuir*, 2005, **21**, 11780-11787.
58. Y. Ni, K. Mi, C. Cheng, J. Xia, X. Ma and J. Hong, *Chemical Communications*, 2011, **47**, 5891-5893.
59. Y. Liu, Y. Li and X.-P. Yan, *Advanced Functional Materials*, 2008, **18**, 1536-1543.
60. F. He, W. Wang, J.-W. Moon, J. Howe, E. M. Pierce and L. Liang, *Acs Applied Materials & Interfaces*, 2012, **4**, 4373-4379.
61. C.-L. Lin, C.-F. Lee and W.-Y. Chiu, *Journal of Colloid and Interface Science*, 2005, **291**, 411-420.
62. C. Liu, R. Bai and Q. San Ly, *Water Research*, 2008, **42**, 1511-1522.
63. Z. Reddad, C. Gerente, Y. Andres and P. Le Cloirec, *Environmental Science & Technology*, 2002, **36**, 2067-2073.
64. G. Zhao, J. Li, X. Ren, C. Chen and X. Wang, *Environmental Science & Technology*, 2011, **45**, 10454-10462.

Figure captions

Figure 1.	FTIR spectra of PVF, PVF-g-GAM-20 and PVF-g-GAA-20.
Figure 2.	Pore size distributions of PVF, PVF-g-GAM-20 and PVF-g-GAA-20.
Figure 3.	FE-SEM images of (a) PVF, (b) PVF-g-GAM-20, (c) PVF-g-GAA-20 (d) PVF-g-GAA-20-Cu and (e) PVF-g-GAA-20-Pb, b-2, c-2, d-2, e-2 are enlarged view of local structure in b-1, c-1, d-1, e-1, respectively.
Figure 4.	Nitrogen content and hydrolysis degree of PVF-g-GAA-20 ([GA]/[OH]=1/4, [AM]/[OH]/[Ce(IV)]/[H+] = 20/1/0.1/0.01) as a function of hydrolysis time (1 M NaOH, 60^{o}C).
Figure 5.	Water absorption amount of PVF sponges in deionized water with contact time.
Figure 6.	Adsorption kinetic curves of PVF-g-GAA-20 in single ion system, Cu^{2+}, Pb^{2+}, and Cd^{2+} solutions (20^{o}C, 2.5 mM, pH=5.11), (b) the corresponding fitted kinetic curves.
Figure 7.	Adsorption procedure of PVF-g-GAA-20 in Cu^{2+} solution (c_0=2.5 mM, pH=5.11).
Figure 8.	Influence of solution pH values on (a) adsorption capacities for metal ions (20^{o}C, 2.5 M) and (b) Zeta potential of PVF-g-GAA-20.
Figure 9.	Saturated adsorption capacities of PVF-g-GAA-20 in (a) Cu^{2+}, (b) Pb^{2+} and (c) Cd^{2+} solutions with various concentrations (20^{o}C, pH=5.11) with fitted curves using Langmuir model and Freundlich model.
Figure 10.	Influence of binary metal ions on the adsorption capacities of

	PVF-g-GAA-20, (a) Cu^{2+}/Pb^{2+} mixture, (b) Cu^{2+}/Cd^{2+} mixture and (c) Pb^{2+}/Cd^{2+} mixture.
Figure 11.	Influence of ionic strength (adjust using NaCl solution) on the adsorption capacities of PVF-g-GAA-20 for $Cu^{2+}$and Pb^{2+} (C_0 = 2.5 mM, pH=5.11).
Figure 12.	Desorption procedure of PVF-g-GAA-20-Cu^{2+} in HCl aqueous solution ($c_{0(HCl)}$ = 0.1 M, 30 mL).
Figure 13.	Adsorption capacities of PVF-g-GAA-20 for Cu^{2+}, Pb^{2+} and Cd^{2+} at different regeneration cycles.
Figure 14.	(A) XPS spectra for PVF-g-GAA-20 after adsorption of Cu^{2+} and Pb^{2+}; (B) FTIR spectra and (C) enlarged view of SEM images of (a) PVF-g-GAA, (b) PVF-g-GAA-20-Cu and (c) PVF-g-GAA-20-Pb.
Table 1.	Related parameters from the kinetics equation, Langmuir and Freundlich adsorption isotherm models fitting to the experimental results
Table 2.	Adsorption performance of PVF-g-GAA-20 for toxic metal ions and comparison with reported in literature
Table of contents (TOC)	

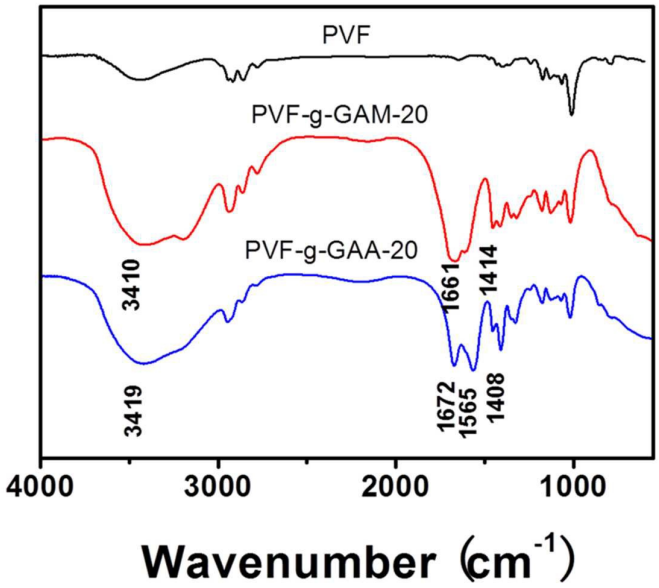

Figure 1. FTIR spectra of PVF, PVF-g-GAM-20 and PVF-g-GAA-20.

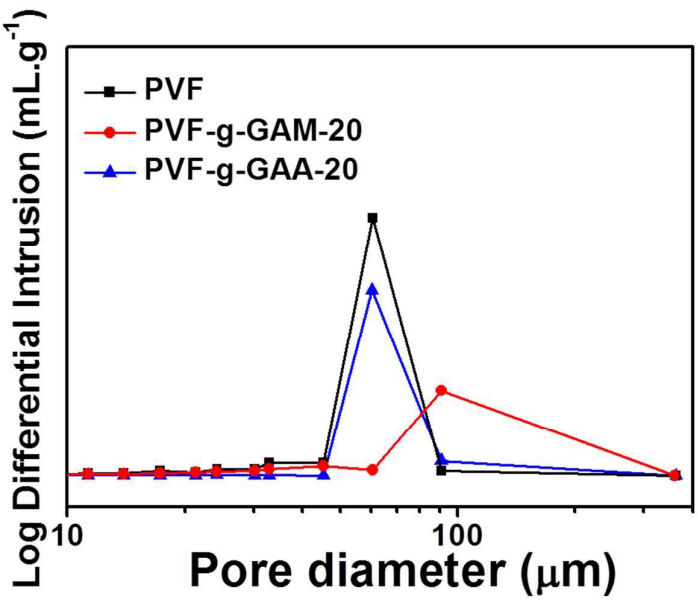

Figure 2. Pore size distributions of PVF, PVF-g-GAM-20 and PVF-g-GAA-20.

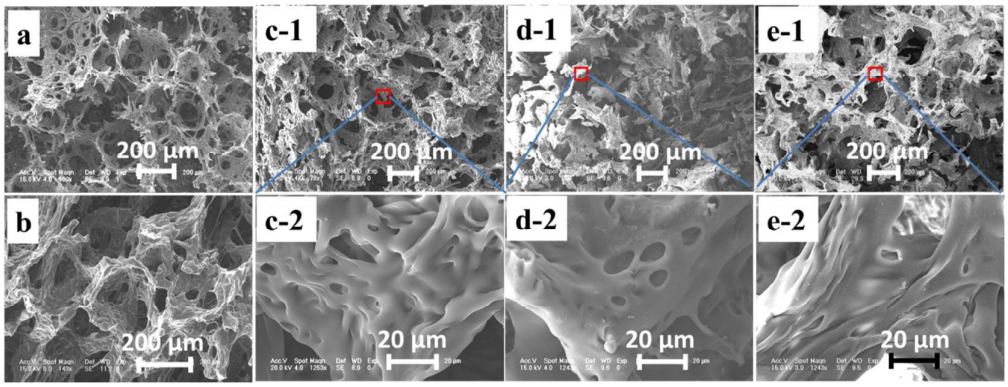

Figure 3. FE-SEM images of (a) PVF, (b) PVF-g-GAM-20, (c-1) PVF-g-GAA-20 (d-1) PVF-g-GAA-20-Cu and (e-1) PVF-g-GAA-20-Pb, c-2,, d-2, e-2 and are enlarged view of local structure in b-1, c-1, d-1, e-1, respectively.

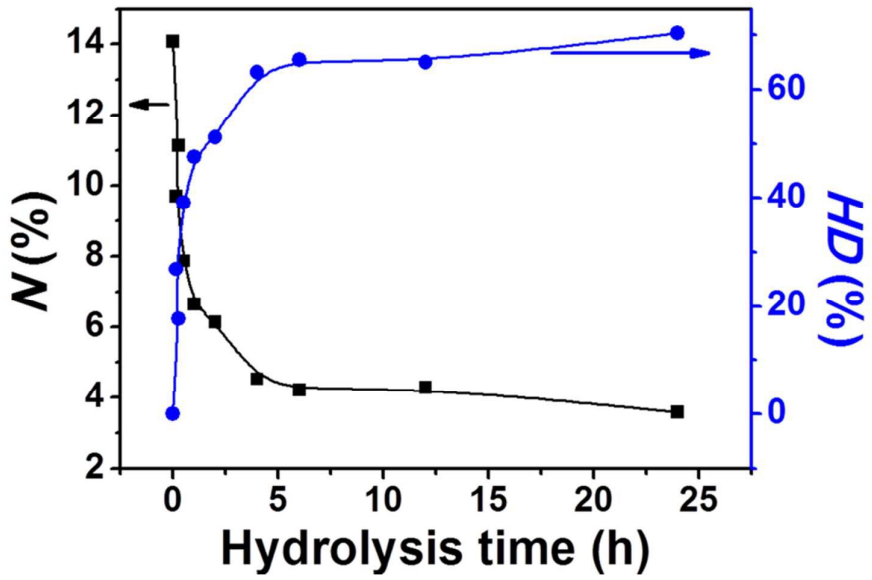

Figure 4. Nitrogen content and hydrolysis degree of PVF-g-GAA-20 ([GA]/[OH]=1/4, [AM]/[OH]/[Ce(IV)]/[H^+] = 20/1/0.1/0.01) as a function of hydrolysis time (1 M NaOH, 60^{o}C).

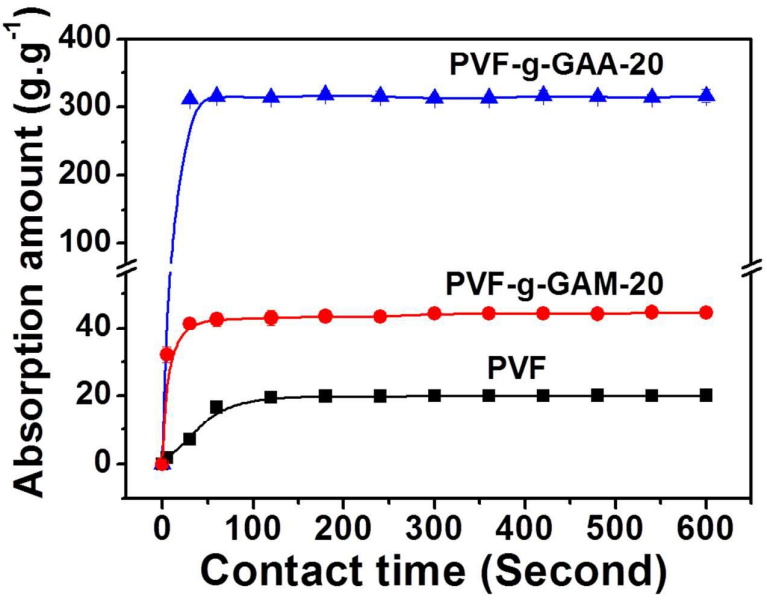

Figure 5. Water absorption amount of PVF sponges in deionized water with contact time.

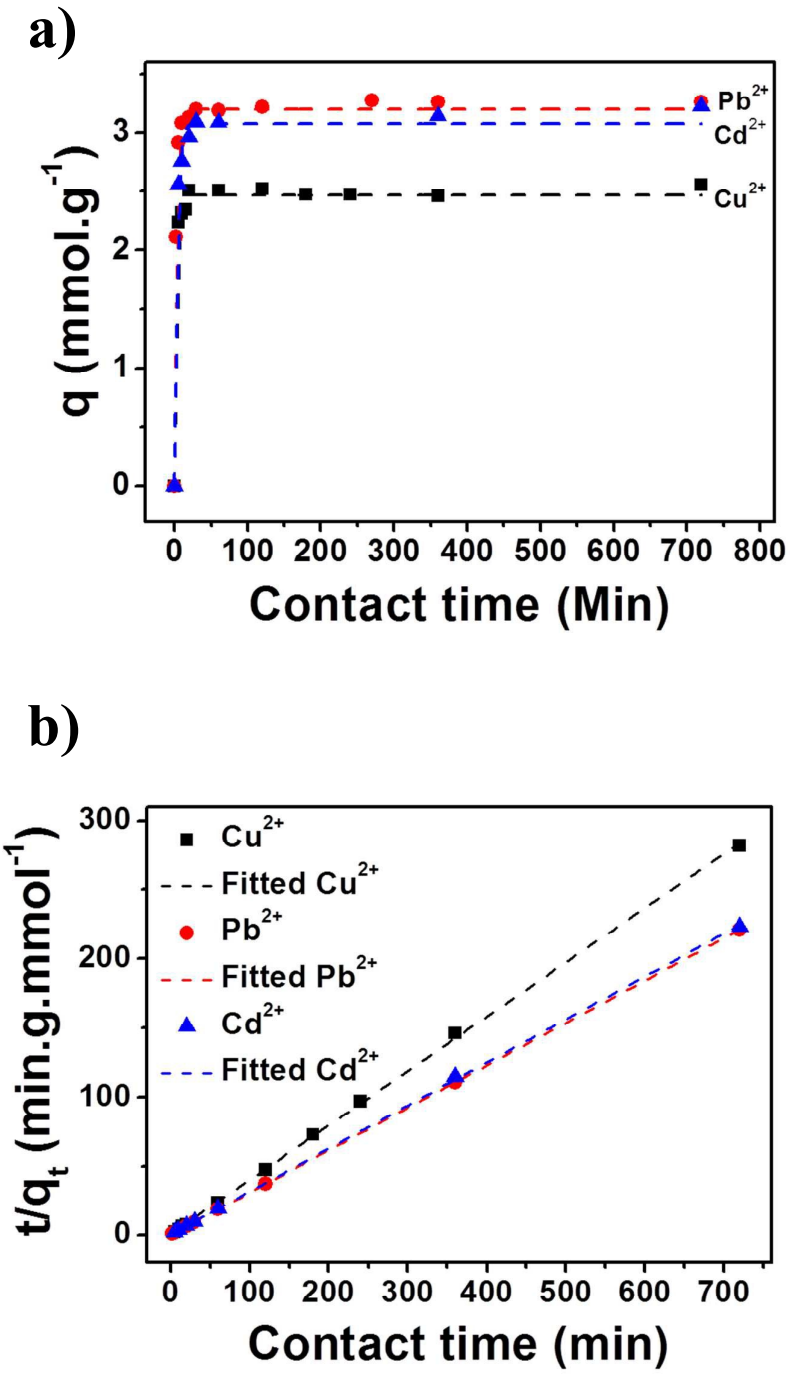

Figure 6. (a) Adsorption kinetic curves of PVF-g-GAA-20 in single ion system, Cu^{2+}, Pb^{2+}, and Cd^{2+} solutions (20°C, 2.5 mM.L^{-1}, pH=5.11), (b) the corresponding fitted kinetic curves.

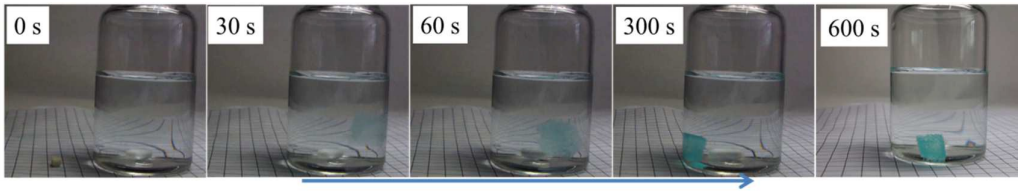

Figure 7. Adsorption procedure of PVF-g-GAA-20 in Cu^{2+} solution at different time (c_0 = 2.5 mM.L^{-1}, pH = 5.11).

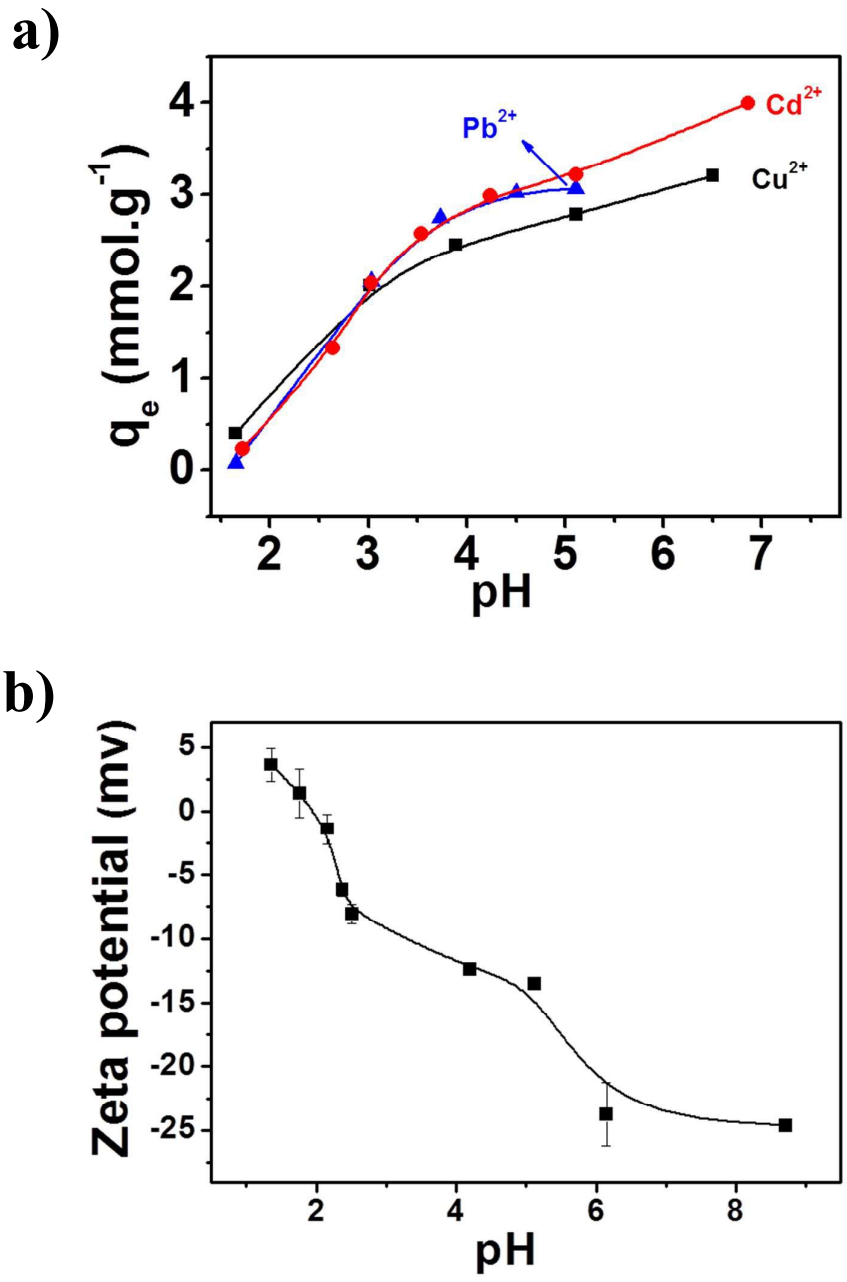

Figure 8. Influence of solution pH values on (a) adsorption capacities for metal ions (20^oC, C_0 = 2.5 mmol.L^{-1}) and (b) Zeta potential of PVF-g-GAA-20.

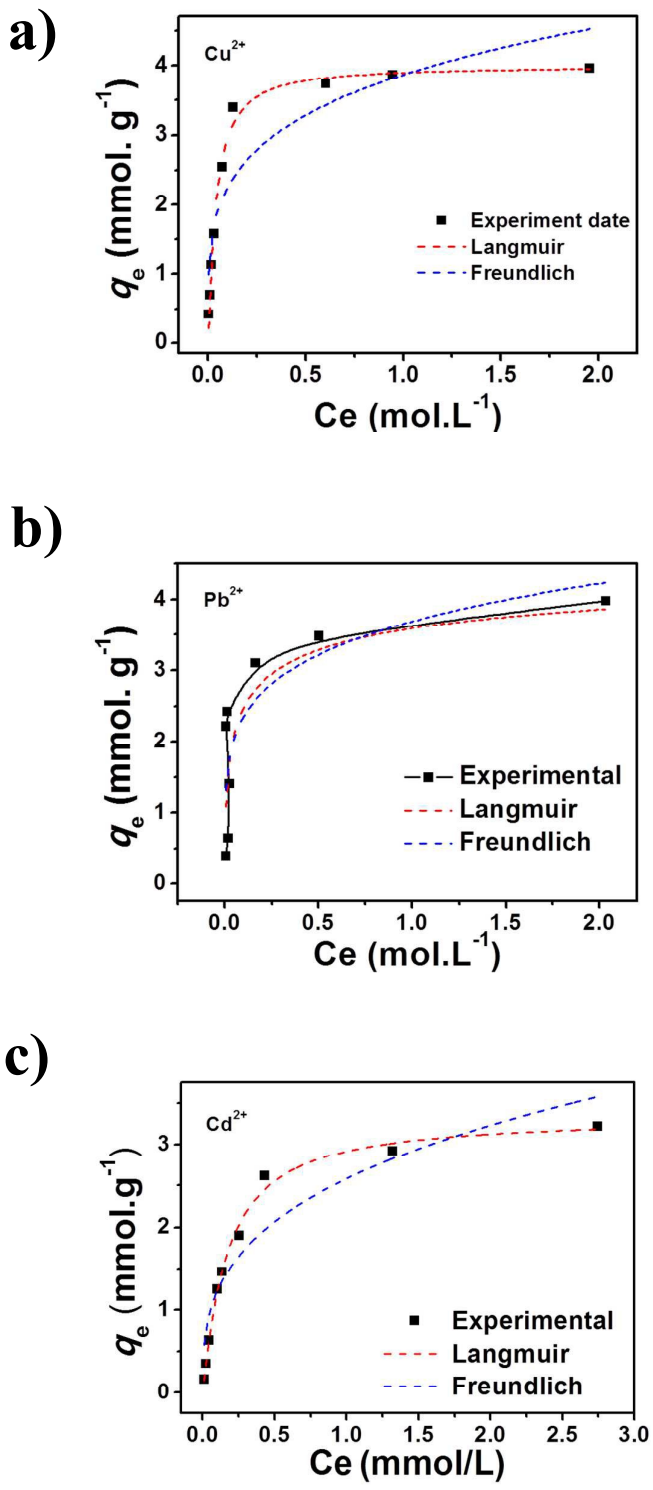

Figure 9. Saturated adsorption capacities of PVF-g-GAA-20 in (a) Cu^{2+}, (b) Pb^{2+} and (c) Cd^{2+}solutions with various concentrations (20°C, pH=5.11) with fitted curves using Langmuir model and Freundlich model.

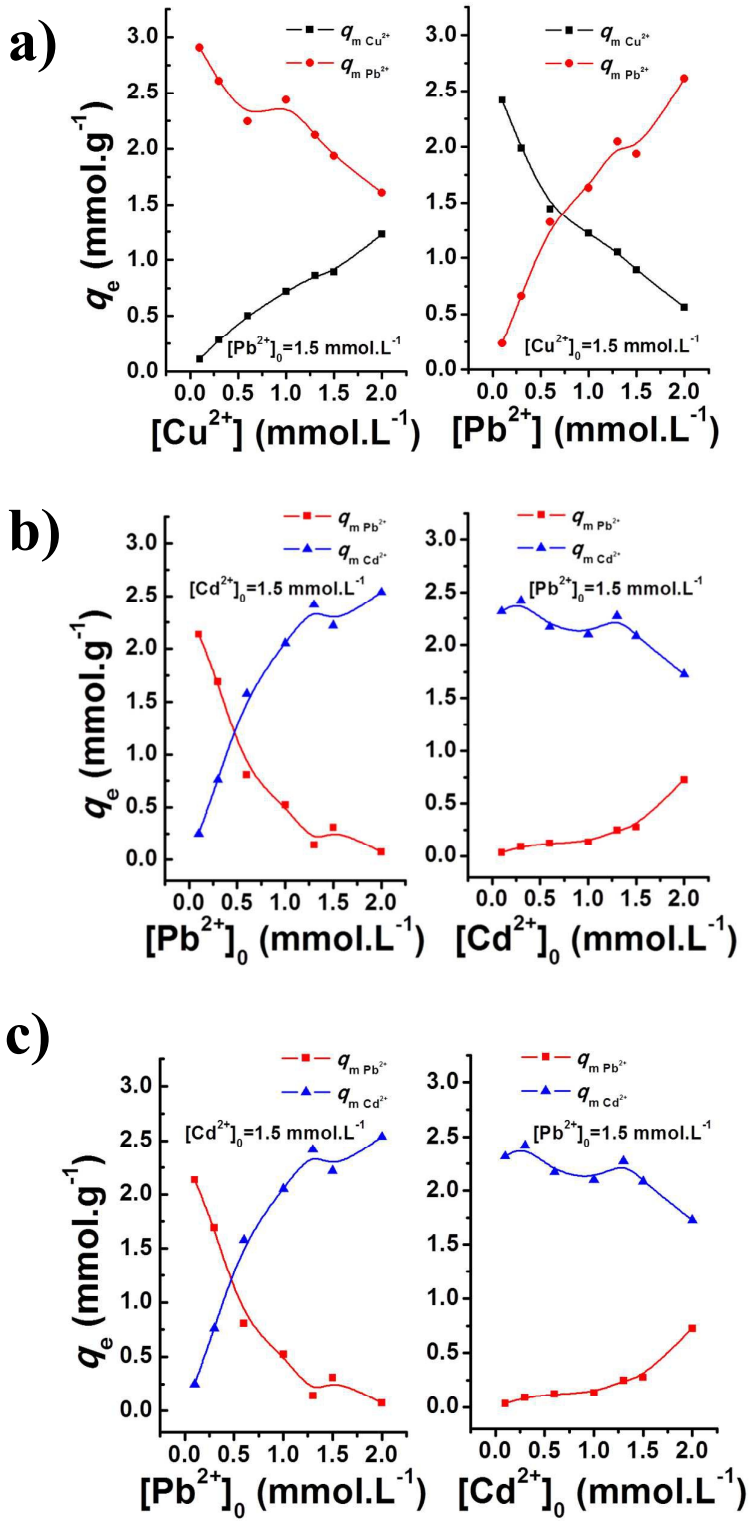

Figure 10. Influence of binary metal ions on the adsorption capacities of PVF-g-GAA-20, (a) Cu^{2+}/Pb^{2+} mixture, (b) Cu^{2+}/Cd^{2+} mixture and (c) Pb^{2+}/Cd^{2+} mixture.

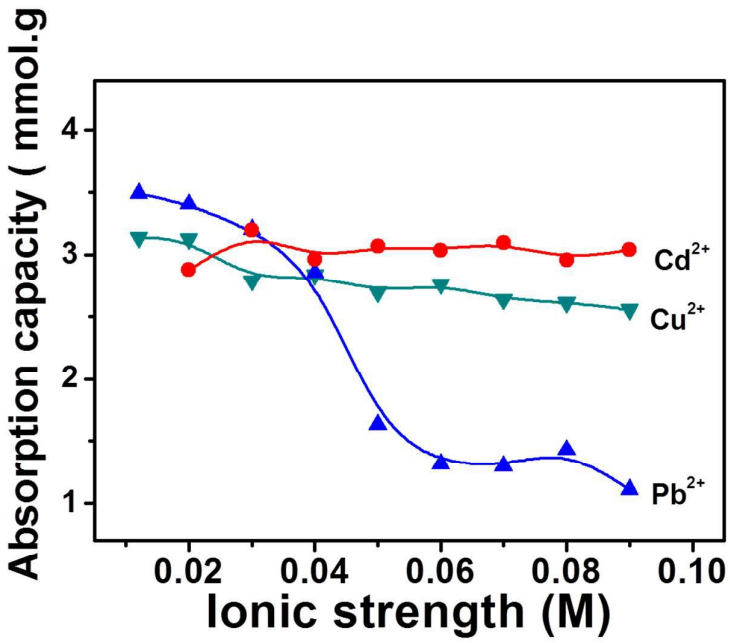

Figure 11. Influence of ionic strength (adjust using NaCl) on the adsorption capacities of PVF-g-GAA-20 for Cu^{2+}, Pb^{2+} and Cd^{2+} (C_0 = 2.5 mM, pH=5.11).

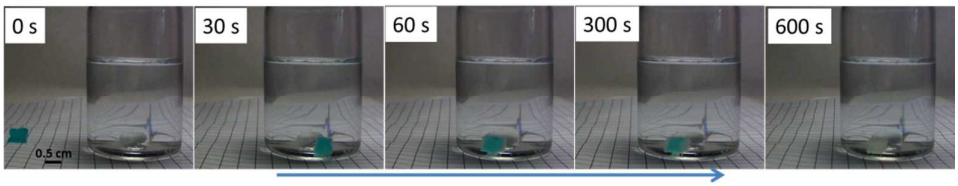

Figure 12. Desorption procedure of PVF-g-GAA-20-Cu^{2+} in HCl aqueous solution ($c_{0(HCl)}$ = 0.1 M, 30 mL).

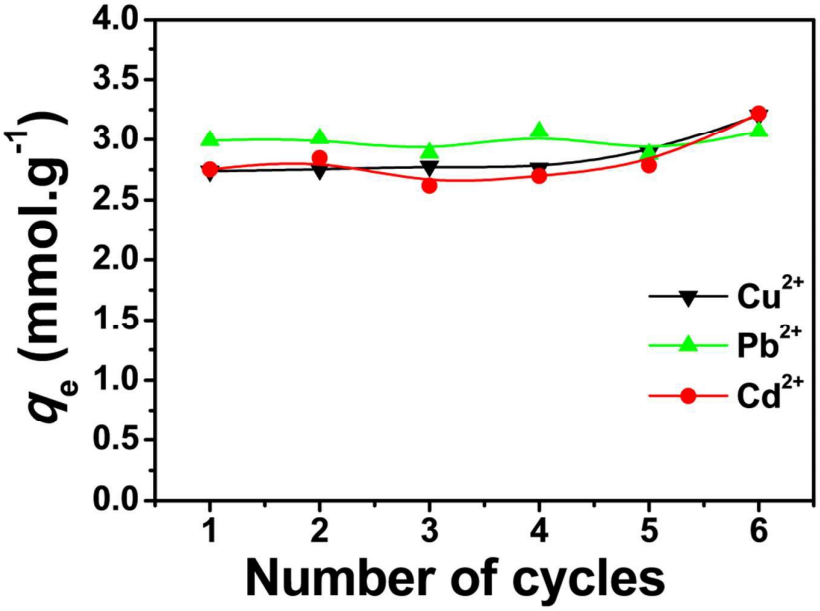

Figure 13. Adsorption capacities of PVF-g-GAA-20 in Cu^{2+}, Pb^{2+} and Cd^{2+} solutions at different cycles.

A)

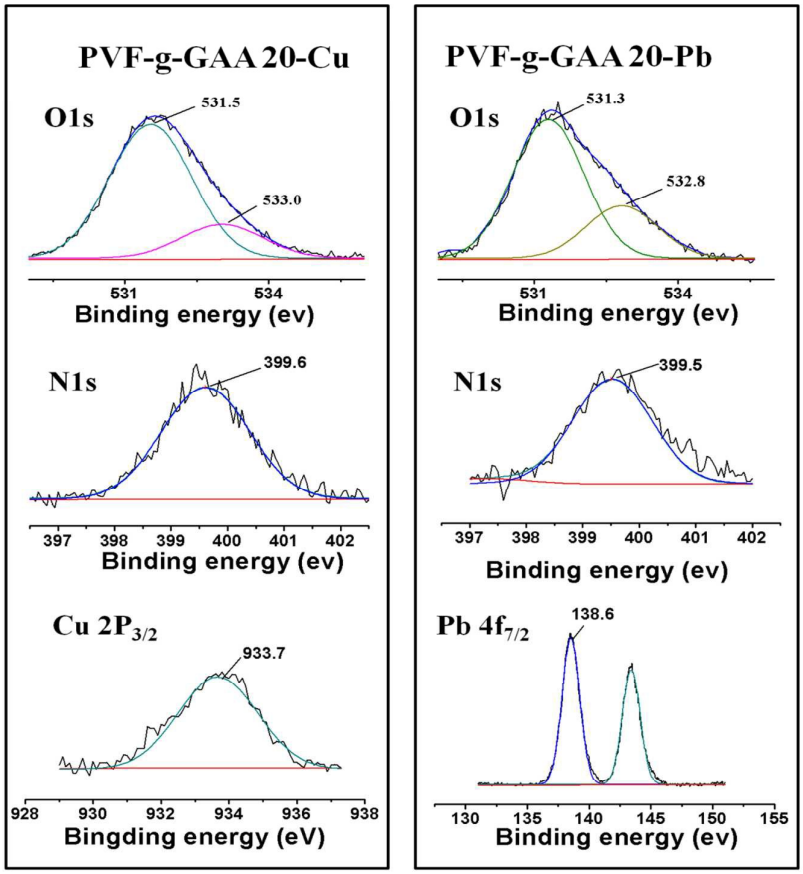

B)

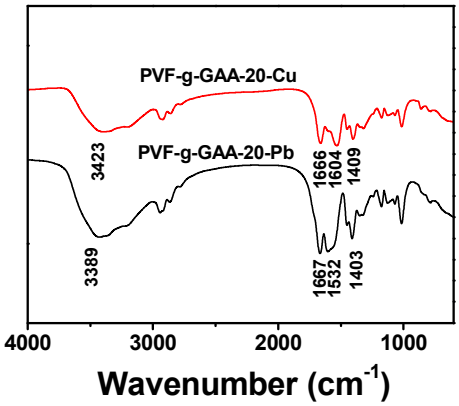

C)

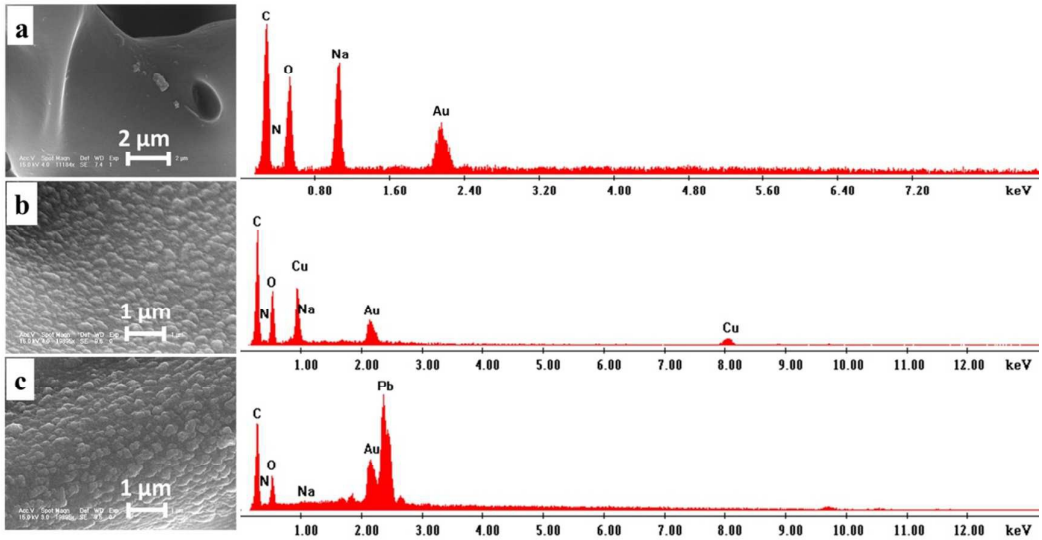

Figure 14. A) XPS spectra for PVF-g-GAA-20 after adsorption of Cu^{2+} and Pb^{2+}; B) FTIR spectra and C) enlarged view of SEM images and correspondingly EDAX mapping of (a) PVF-g-GAA, (b) PVF-g-GAA-20-Cu and (c) PVF-g-GAA-20-Pb.

Table 1. Related Parameters from the Kinetics Equation, Langmuir and Freundlich Adsorption Isotherm Models Fitting to the Experimental Results

metal ions	experi-mental	pseudo-first order kinetic equation fitting			pseudo-second order kinetic equation fitting			Freundlich model			Langmuir model		
	q_e mmol·g^{-1}	q_e mmol·g^{-1}	K_1 min^{-1}	R^2	q_e mmol·g^{-1}	K mmol·min^{-1}	R^2	K_F mmol$^{1-1/n}$·L$^{1/n}$·g^{-1}	1/n	R^2	q_m mmol·g^{-1}	K L·mmol^{-1}	R^2
Cu^{2+}	2.50	2.47	0.45	0.9907	2.56	0.153	1.0000	3.87	0.235	0.8271	4.00	0.027	0.9885
Pb^{2+}	3.26	3.20	0.52	0.9963	3.15	0.101	1.0000	3.69	0.196	0.6152	3.97	0.054	0.9770
Cd^{2+}	3.15	3.07	0.33	0.9879	3.10	0.104	0.9998	2.58	0.322	0.8805	3.34	0.146	0.9929

T**able 2.** Adsorption Performance of PVF-g-GAA-20 for Toxic Metal Ions and Comparison with Reported in Literature

Adsorbents	Absorbate	Adsorption capacity (mmol. g^{-1})	Time to reach q_e (min)	Condition	References
PVF-g-GAA-20	Cu^{2+}, Pb^{2+} and Cd^{2+}	~3.3-4.0	~ 10	pH=5.5, RT	**This work**
Fe3O4@PMAA composite	Cu^{2+}, Pb^{2+}, Cr^{3+}, Cd^{2+}	~ 1.0-3.5	——	pH=5.0, RT	[11]
DETA modified sorbents	Cu^{2+} and Cd^{2+}	~ 0.2	~30	pH=3~5, RT	[12]
Core–shell microspheres	Pb^{2+}	~ 1.1	~ 10	pH=5, RT	[15]
GO/CMC monoliths	Cu^{2+}, Cd^{2+} and Pb^{2+}	~ 0.3- 1.2	——	——	[19]
Graphene oxide–chitosan composite hydrogels	Cu^{2+}	~ 2	~10	pH= 5.0, RT	[23]
Cation-exchange Resin-Supported PEI	Cu^{2+}	~ 1.5	~ 240	pH=6.0, RT	[30]
PASP resin	Cu^{2+} and Cd^{2+}	~ 1.2-1.4	~ 40	pH=5, RT	[31]
Aminated Polyacrylonitrile Fibers	Cu^{2+}	~0.3-0.5	~120	pH=4.5, RT	[33]
Nanocrystalline Cellulose	Cu^{2+}	~0.3-0.5	~120	pH=4.0 ± 0.2, RT	[32]
Polyacrylonitrile Nanofiber Mats	Cu^{2+}, Pb^{2+}, Cr^{3+}	~1.5-3.3	~1200	pH> 56, 25^{o}C	[34]
Xylan-Rich Hemicelluloses hydrogel	Pb^{2+}, Cd^{2+}	~ 4.1	~60	pH=3.5-6.5, RT	[36]
Urchin-like Ni–P microstructures	Pb^{2+} and Cd^{2+}	~ 0.8-1.11	~ 10	——	[57]

L-Cysteine functionalized MCNTs	Cd^{2+}	~ 0.4	60	pH=5.5	[59]

TOC